Available online at www.sciencedirect.com
SCIENCE DIRECT
Journal of Power Sources 151 (2005) 32–42
JOURNAL OF POWER SOURCES
www.elsevier.com/locate/jpowsour

Preferential oxidation of CO in a H_2-rich stream over CuO/CeO_2 and $CuO/(Ce,M)O_x$ (M = Zr, Tb) catalysts

A. Martínez-Arias [a,*], A.B. Hungría [a], M. Fernández-García [a], J.C. Conesa [a], G. Munuera [b]

[a] *Instituto de Catálisis y Petroleoquímica, CSIC, C/ Marie Curie, Campus Cantoblanco, 28049 Madrid, Spain*
[b] *Departamento de Química Inorgánica, Universidad de Sevilla, 41092 Sevilla, Spain*

Accepted 4 February 2005
Available online 25 April 2005

Abstract

Catalysts with the same copper oxide loading supported on cerium oxide and Ce–M (M = Zr or Tb) mixed oxides are examined with respect to their performance for preferential oxidation of CO (CO-PROX) in a H_2-rich stream. The catalytic activity results are analysed in combination with *operando*-DRIFTS tests done under similar conditions and characterization results obtained by XRD, XPS and XAFS techniques. The presence of essentially highly dispersed CuO entities strongly interacting with the corresponding supports and differing in their dispersion degree is evidenced by these techniques. The catalytic activity results reveal significant support effects affecting the conversion of either CO or H_2 as well as the selectivity for the CO-PROX process. These are explained on the basis of differences in the interfacial redox activities of the corresponding copper oxide-support contacts, while copper oxide particle size effects are proposed to be relevant to explain overall CO-PROX selectivities obtained.
© 2005 Elsevier B.V. All rights reserved.

Keywords: Copper oxide/ceria–zirconia–terbia catalysts; CO-PROX; XPS; XAFS; XRD; Operando-DRIFTS

1. Introduction

Hydrogen production from hydrocarbons has been proposed as the most efficient process to obtain such fuel for its use by proton-exchange membrane fuel cells (PEMFC). However, the gas produced after reforming of hydrocarbon fuels followed by water gas-shift (WGS) processes employed for this purpose still presents in most cases (typical composition: 45–75 vol.% H_2, 15–25 vol.% CO_2, 0.5–2 vol.% CO, a few vol.% H_2O and traces of unconverted fuel [1]), a relatively high CO concentration that disallows efficient handling of the fuel by the Pt alloy anode usually employed in the PEMFC. Preferential (or selective) oxidation of CO (PROX process) has been recognized as one of the most straightforward and cost-effective methods to achieve acceptable CO concentrations (below ca. 100 ppm) [1–4].

Different types of catalysts have shown their efficiency for the PROX process. These can be classified into three general groups as a function of their nature and/or consequent catalytic properties. The first one involves supported noble metal catalysts (mainly Pt ones) and follows from first developments done by Engelhard researchers in the context of processes related to ammonia production [1,5]. Although nowadays operating PROX systems include this type of catalysts, they present the main drawback (apart from their cost) of their relatively low selectivity for the process (that could probably be enhanced with the use of certain promoters and/or upon appropriate selection of the support [6,7]) at their operating temperature (between 423 and 473 K), which makes necessary including interstage cooling operations to avoid extensive heating as a consequence of the exothermicity of the reactions involved [1,8]. A second group involves supported gold (or oxidized gold) catalysts, well known for their outstanding performance for CO oxidation [1,9,10]. These systems show a high activity for the PROX process

* Corresponding author.
E-mail address: amartinez@icp.csic.es (A. Martínez-Arias).

0378-7753/$ – see front matter © 2005 Elsevier B.V. All rights reserved.
doi:10.1016/j.jpowsour.2005.02.078

with a better match between their activity window and the PEMFC anode operating temperature (353–403 K). They present, however, the drawback of their poor resistance to the presence of CO_2 and H_2O in the reactant mixture [1,9,10]. The third group under research is related to formulations based on closely interacting copper oxide and ceria (or structurally related cerium-containing mixed oxides). These have shown promising properties in terms of activity, selectivity and resistance to CO_2 and H_2O, while being probably most interesting from an economical point of view [1–4].

The particular ability of the latter class of catalysts for the PROX or related processes has been essentially attributed to the exceptional redox properties achieved by interfacial sites upon establishment of interactions between both catalyst components [2,3,11,12]. This has allowed establishing correlations between redox and catalytic properties of the system, strongly indicating that the reaction mechanism is essentially of a Mars-van Krevelen type [3,12]. As shown in previous reports, the redox properties of CuO_x–$(Ce,M)O_x$ contacts strongly depend on the nature as well as the structural/morphological properties of both CuO_x and $(Ce,M)O_x$ entities [11–13]. On the other hand, previous extensive investigations in the three-way catalysts field have shown the benefits of substituting simple ceria by ceria-related mixed oxides (in particular Ce–Zr, but also Ce–Tb ones [14]) as promoter in the catalysts formulation, which has mainly been attributed to the enhanced redox properties (basically related to the higher oxygen mobility) of the latter. Within this context, the present work aims to get deeper insights into such properties and to analyse support effects in modified formulations. For this purpose, $CuO/(Ce,M)O_x$ catalysts in which the copper loading is kept constant, but the nature of the support is changed (CeO_2 and mixed oxides of Ce–Zr and Ce–Tb, prepared by microemulsion methods in order to get optimum characteristics in terms of compositional and structural/morphological homogeneity, being employed; a detailed characterization of the supports employed can be found elsewhere [15–17]) are examined with respect to their catalytic performance for the CO-PROX process (analysed with both a conventional catalytic reactor and by *operando*-DRIFTS spectroscopy). In turn, these results in combination with characterization ones obtained with XRD, XPS and XAFS techniques are used in an attempt to establish structure/activity relationships.

2. Experimental

The CeO_2 and Ce–M (M = Zr or Tb) supports were prepared by precipitation within a reverse microemulsion. For this, two microemulsions of similar characteristics containing aqueous phases prepared by dissolving nitrate salts of Ce (or Ce and Zr or Tb; nominal atomic ratios employed were Ce/Zr = 1 and Ce/Tb = 4 or 1) for the first and tetramethylammonium hydroxyde pentahydrate for the second were mixed; *n*-heptane was used as organic solvent, Triton X-100 (Aldrich) as surfactant and hexanol as co-surfactant in the microemulsions. Following centrifugation, decanting and rinsing of the resulting solid with methanol, it was dried at 383 K for 24 h and finally calcined under air at 773 K for 2 h. Details of the preparation parameters employed during the synthesis of these supports can be found elsewhere [15–18]. The copper oxide catalyst supported on CeO_2, Ce–Zr or Ce–Tb mixed oxides was prepared by incipient wetness impregnation of the corresponding support using an aqueous solution of $Cu(NO_3)_2{\cdot}3H_2O$ (to give a final copper load of 1 wt.%, representing ca. 157 μmol of Cu/g of catalyst). The resulting material was dried overnight at 383 K and subsequently calcined under air at 773 K for 2 h. The nomenclature used for these catalysts as well as their main textural or compositional properties are summarized in Table 1.

The catalysts calcined in situ (under diluted oxygen at 773 K) were tested for their activity under an atmospheric pressure flow (using mass flow controllers to prepare the mixture) of 1% CO, 1.25% O_2 and 50% H_2 (Ar balance), at a rate of 1×10^3 cm^3 min^{-1} g^{-1} (roughly corresponding to 80,000 h^{-1} GHSV) and using a heating ramp of 5 K min^{-1} up to 573 K; at the end of the test, the catalysts were examined during cooling under the same flow using a –5 K min^{-1} ramp, showing generally the presence of relatively narrow hysteresis loops. Analysis of the feed and outlet gas streams was done by gas infrared (Perkin-Elmer FTIR spectrometer model 1725X, coupled to a multiple reflection transmission cell, Infrared Analysis Inc., "long-path gas minicell", 2.4 m path length, ca. 130 cm^3 internal volume), while a paramagnetic analyser (Servomex 540 A) was used to analyse the O_2 concentration. No products other than those resulting from CO or H_2 combustion (i.e. CO hydrogenation ones like methane, for instance) were detected in the course of the runs.

Operando-DRIFTS analysis of the samples was carried out using a Bruker Equinox 55 FTIR spectrometer fitted with an MCT detector. The DRIFTS cell (Harrick) was fitted with CaF_2 windows and a heating cartridge that allowed samples to be heated to 773 K. Samples of ca. 100 mg were calcined in situ (in a similar way as employed for the catalytic tests) and then cooled to 298 K under diluted oxygen before introducing the reaction mixture and heating in a stepped way, recording one spectrum (average of 50 scans at 4 cm^{-1} resolution) after stopping the ramp every 10 K when the signal of the paramagnetic analyser (coupled on-line for O_2 analysis at the outlet of the DRIFTS cell) becomes constant. The gas mixture (either joint CO and H_2 oxidation 1% CO + 1.25% O_2 + 50% H_2 in Ar or individual CO or H_2 oxidation reactions 1% CO + 1.25% O_2 or 50% H_2 + 1.25% O_2, Ar balance in any case, were examined in this case) was prepared using mass flow controllers with ca. 100 cm^3 min^{-1} passing through the catalyst bed at atmospheric pressure, which corresponds to conditions similar to those employed for the reaction tests.

X-ray photoelectron spectra (XPS) were recorded with a Leybold–Heraeus spectrometer equipped with an EA-200 hemispherical electron multichannel analyzer (from Specs) and a 120 W, 30 mA Mg Kα X-ray source. A computer was used for controlling the instrument and recording of the

Table 1
Summary of compositional and textural characteristics of the catalysts

Catalyst	Support used	Ce/M atomic ratios[a]	Cu loading (wt.%)	S_{BET} ($m^2\ g^{-1}$)
CuC	CeO_2		1	92
CuCZ	Ce–Zr mixed oxide	Ce/Zr = 1.08	1	96
CuCT1	Ce–Tb mixed oxide	Ce/Tb = 1.10	1	95
CuCT4	Ce–Tb mixed oxide	Ce/Tb = 3.93	1	104

[a] Values determined from ICP–AES chemical analysis.

spectra. Ar^+-etching treatments were carried out with a current of 6 mA and an acceleration voltage of 3.5 kV (ion current, 8 μA). This gave a sputtering yield rate of ca. 12 Å min^{-1}, according to a calibration made using a standard Ta_2O_5 thin film electrochemically grown on a Ta foil; the ion damage (penetration) depth in these conditions was estimated as ca. 5 nm by TRIM-90 using Monte Carlo standard calculations [19]. The sample (0.2 mg) was slightly pressed into a small (4 mm × 4 mm) pellet and then mounted on a sample rod and introduced into the pretreatment chamber, where it was outgassed at 473 K for 2–3 h, until a pressure of less than 2×10^{-8} Torr was achieved, the sample then being reoxidized under 1 Torr of O_2 at the same temperature. Subsequently, it was reduced under 1 Torr CO at 300 K and then further outgassed at 473 K. From this point, the sample was either treated under 1 Torr CO at 300 K or reoxidized with 1 Torr O_2 doses up to 473 K. Following each treatment, the sample was moved into the ion-pumped analysis chamber, where it was further outgassed until a pressure less than 2×10^{-9} Torr was attained (2–3 h). This low pressure was maintained during all the data acquisition by ion pumping of the chamber. After each treatment, XP spectra in the relevant energy windows were collected for 20–90 min, depending on the peak intensities, at a pass energy of 44 eV (1 eV = 1.602×10^{-19} J) which is typical of high-resolution conditions. The intensities were estimated by calculating the integral of each peak after subtraction of an S-shaped Shirley-type background with the help of UNIFIT for Windows (Version 3.2) software [20]; atomic ratios were then derived using the appropriate experimental sensitivity factors. All binding energies (BE) were referenced to the adventitious C1s line at 284.6 eV [21]. This reference gave BE values with an accuracy of ±0.1 eV; the peak u‴ characteristic of Ce^{4+} was, thus, obtained at 917.0 ± 0.1 eV. In the case of Ce(3d) spectra, factor analysis (also known as principal component analysis) was used to calculate the Ce^{3+}/Ce^{4+} ratios in each set of spectra recorded, using the methodology developed in a previous work [22].

XAFS measurements were performed on Station 9.3 at the Daresbury Laboratory (Warrington, UK), equipped with a Pd-coated plane mirror and a Si(2 2 0) double crystal monochromator set at 50% harmonic rejection detune. Data were collected at the Cu K-edge in fluorescence mode using a 13-element Ge solid-state detector with semi automatic windowing and dead time correction. The sample was precalcined under diluted oxygen flow at 773 K and then, after cooling to room temperature under the same flow, taken out from the treatment cell and positioned at ca. 45° to the incident beam in order to maximize the solid angle seen by the detector situated perpendicular to the beam. A total of 12 scans were recorded with a total accumulation time of 2.5 h. Correction due to potential self-absorption effects was made on the basis of the work of Schroeder et al. [23]. The energy scale was calibrated with the measurement of a copper foil and giving a value of 8979.0 eV to the first inflection point.

Powder XRD patterns of the samples were recorded on a Seifert XRD 3000P diffractometer using nickel-filtered Cu Kα radiation operating at 40 kV and 40 mA, using a 0.02° step size and 10 s counting time per point. Analysis of the diffraction peaks was done with the computer program ANALYZE Rayflex Version 2.293.

3. Results and discussion

3.1. Characterization of the catalysts

X-ray diffractograms of the catalysts are shown in Fig. 1. The diffraction peaks observed are similar to those detected for the corresponding supports, with no hint of copper-containing phases being detected; the peaks are in any of the cases indexable according to the presence of the cubic fluorite phase, as expected for this type of oxides [14–18]. The peaks have been analysed by means of Williamson–Hall plots, following an approach similar to that employed by Zhou and

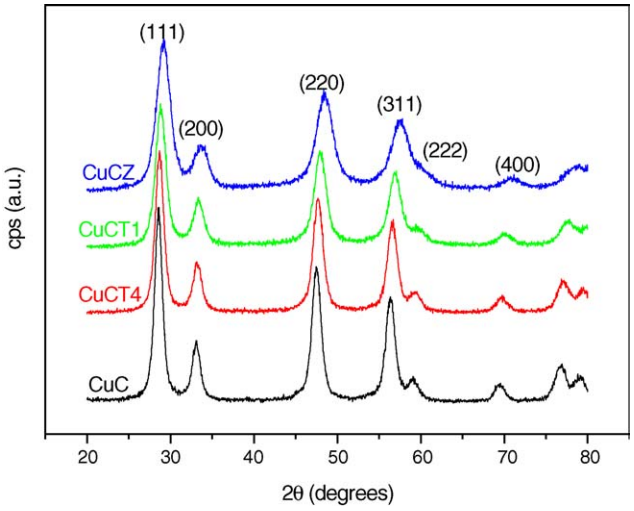

Fig. 1. X-ray diffractograms of the indicated samples.

Table 2
Summary of bulk morphological/structural characteristics of the samples extracted from XRD as well as from HREM and Raman analyses (see text)

Sample	Lattice parameter (Å)	rms microstrain	Particle size (nm)[a]	Phase[b]
CuC (CeO_2)	5.413 (5.412)	2.58×10^{-3} (1.91×10^{-3})	8.3 (7.7)	Cubic fluorite
CuCZ ($Ce_{0.5}Zr_{0.5}O_2$)	5.313 (5.308)	5.67×10^{-3} (3.65×10^{-3})	5.0 (4.5)	Tetragonal t″
CuCT1 ($Ce_{0.5}Tb_{0.5}O_{2-x}$)[c]	5.368 (5.367)	2.53×10^{-3} (3.33×10^{-3})	6.1 (6.0)	Cubic fluorite
CuCT4 ($Ce_{0.8}Tb_{0.2}O_{2-y}$)[c]	5.393 (5.392)	1.81×10^{-3} (3.55×10^{-3})	7.2 (7.4)	Cubic fluorite

Values in parentheses correspond to the corresponding supports.

[a] More or less rounded morphologies are observed for the nanoparticles, which form in turn aggregates in the micron size for all the samples, by HREM [15–17].

[b] On the basis of XRD and Raman results. Note the general selective sensitivity of these techniques for the cationic and anionic sublattices, respectively, in this type of samples; the tetragonality of pseudocubic phase t″ is related to the anionic sublattice, while cationic positions are those corresponding to the cubic fluorite lattice [14,18].

[c] These samples present a certain non-stoichiometry as a consequence of the presence of reduced terbium cations with $(Tb^{3+}/(Tb^{3+} + Tb^{4+})$ ratios of 0.62 and 0.46 being estimated (on the basis of mainly XRD results [15]) for CT4 and CT1 supports, respectively.

Huebner [24], in order to obtain information for particle size and root mean squared microstrain of the samples. The main structural/morphological results extracted from this analysis (including as well results obtained from previous HREM and Raman investigations) are displayed in Table 2. Lattice parameters obtained for the support samples are in agreement with values expected for the corresponding single oxide or mixed oxide samples with the compositions or non-stoichiometry levels (Table 1) detected for them [14–18]. The absence of significant component segregation into separate phases in the mixed oxides is suggested from analysis of the XRD peaks although the relatively large peak width disallows obtaining details in this sense. Nevertheless, previous reports based on multitechnique approaches show the high level of bulk compositional homogeneity and the relatively low particle size dispersion obtained for these oxides [15–17]. On the other hand, the evolution of microstrain values between the support samples reflects, in accordance with a previous report [25], the increase in lattice strain as a consequence of the presence of bulk defects (anionic vacancies for the non-stoichiometric Ce–Tb mixed oxides) or distortions in the oxygen sublattice (for the Ce–Zr mixed oxide) upon introduction of the heterocations in the fluorite lattice. The presence of copper in the catalysts induces minor changes in the bulk characteristics of the materials (Table 1), which indicates (as expected taking into account the preparation method employed) that copper must be essentially located at the surface of the corresponding oxide supports. This has been recently confirmed (on the basis of combined XRD and Raman analysis) for the CuC sample [26]. Small particle size changes are also produced upon introduction of copper that may be related to effects induced during the preparation steps involved in copper impregnation of the supports. In turn, copper-induced changes in microstrain values must be related to modifications in interparticle interactions as a consequence of copper presence at the sample surface and/or to the presence of small portions of copper at subsurface positions of the cubic (or pseudocubic) lattice [26]. It is nevertheless interesting in this respect that the opposite effect is observed for the catalysts supported on Ce–Tb mixed oxides (in which bulk defects are present) and CeO_2 or Ce–Zr mixed oxide.

The absence of copper-related phases in the X-ray diffractograms of Fig. 1 indicates a relatively high dispersion state of such component. This is confirmed by XPS measurements showing Cu/(Ce + M) − M = Zr or Tb, atomic ratios of 0.084, 0.085, 0.088 and 0.073 for CuC, CuCT4, CuCT1 and CuCZ, respectively. The characterization of copper has been carried out by XAFS and XPS techniques. Fig. 2 shows the Cu K-edge XANES spectra of CuC and CuCT1 samples, which display strong similarities between each other. A comparison with a bulk CuO reference and a Cu–ZSM-5 sample, which displays the exclusive presence of isolated Cu^{2+} species [27], provides evidence that Cu is in both samples, mostly inserted in a CuO-type matrix, small differences being most likely related to the relatively high dispersion state of copper in them. This is shown in the bottom of Fig. 2; the comparison of the second derivatives displays modulations at the edge region (8975–9000 eV) peaking at rather close energies in the case of both CuC and CuCT1 samples and the CuO reference, while the isolated Cu^{2+} species showed all such peaks with maxima shifted to higher energy. This difference in the energy location of second derivative peaks between aggregated and isolated species is a constant which has been previously reported by others [28]. The absence of a significant amount of isolated Cu^{2+} species was previously confirmed by EPR for CuC and CuCZ samples, in which only a minor signal related to such species was detected [11]. XPS analysis of the chemical state of copper in CuC and CuCZ samples reveals, in agreement with XAFS results, that Cu in these samples (treated under vacuum at 473 K followed by treatment under O_2 at 473 K) is chemically similar to Cu^{2+} in bulk CuO. This is shown by the positions of the corresponding points in the Wagner type diagram (made up from the energies E_b and E_k observed for the Cu $2p_{3/2}$ and Cu($L_3M_{45}M_{45}$, ^1G) peaks, respectively, and the modified Auger parameter – $\alpha' = E_B + E_K$) displayed in Fig. 3. However, the shift towards a lower value of α' within the dashed line of slope-3 crossing through the reference point for bulk CuO indicates a much smaller extraatomic relaxation of the photohole with respect to such reference, suggesting a relatively strong effect of CuO size and/or of the support interface to the relaxation process [29]. In any case, both XAFS and XPS techniques reveal that copper is fully oxidized (Cu^{2+}

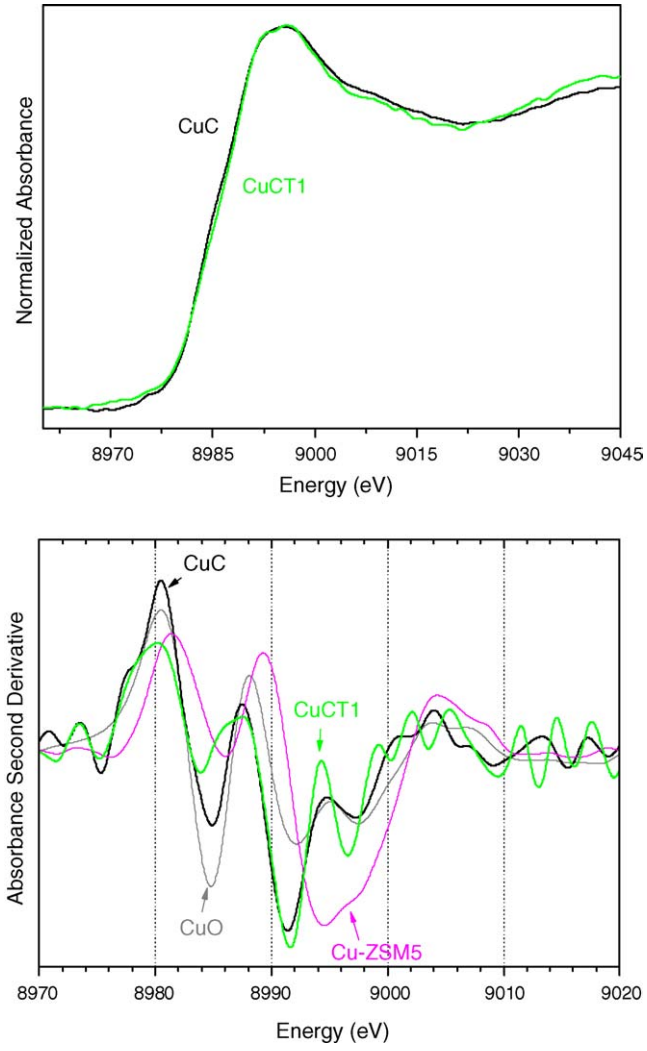

Fig. 2. Cu K-edge XANES spectra of the CuC and CuCT1 samples (top). Second derivative spectra of CuC and CuCT1 compared with those of CuO and Cu^{2+}–ZSM5 references (bottom).

state) in the examined samples and appears essentially in the form of highly dispersed CuO-type entities.

Differences between the samples with respect to the state of copper have been revealed by XPS Ar^+-sputtering experiments. The profile of Cu/(Ce + M) – M = Zr or Tb-atomic ratio evolutions observed for CuC, CuCT1 and CuCZ samples are shown in Fig. 4; the profile observed for CuCT4 (not included in Fig. 4) was fairly similar to that shown by CuC. Analysis of such evolutions can be made by using previously established models [30,31], by which the observed profiles arise from superimposition of curves from dispersed species (responsible of the small initial sharp decline) with that from large particles (for which an initial increase in Cu/(Ce + M), responsible of the observed intermediate maxima, would be expected). On this basis, the observed results indicate that the CuO-type basically present multimodal distributions of CuO particles with the width of such distribution most likely following the order CuC ≈ CuCT4 > CuCT1 > CuCZ1. In turn, overall dispersions of such copper oxide entities is inferred to decrease as CuCZ > CuCT1 > CuCT4 ≈ CuC.

3.2. Catalytic properties

The results of catalytic activity tests under $CO + O_2 + H_2$ are shown in Fig. 5. Several aspects are immediately observed upon analysis of the activity profiles. Thus, significant support effects are revealed that affect to both CO conversion and selective oxidation of CO. Concerning the former, the results show that the activity for CO conversion follows the order CuC > CuCZ ≈ CuCT4 > CuCT1 with the CuC catalyst reaching 100% CO conversion in a relatively narrow temperature window (between 413 and 433 K). With respect to selectivity for the CO PROX process (essentially related to the CO oxidation reaction, taking into account that, as mentioned in the experimental part, CO_2 and H_2O are the only products detected and that possible WGS-related processes must be slow in this type of catalysts for $T <$ ca. 473 K under the conditions employed [32]), the results show lowest overall selectivity levels for the CuCZ catalysts with all of them showing around 40–45% selectivity at maximum CO conversion. Noteworthy, a maximum in the selectivity, particularly apparent for CuC, is observed for all of them at intermediate reaction temperature. Influence of the presence

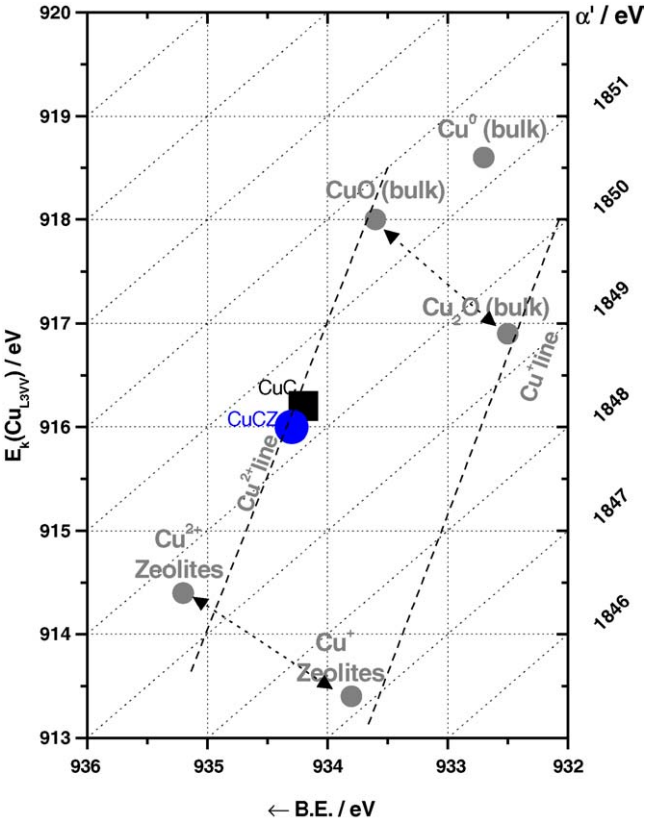

Fig. 3. Wagner diagram showing Cu (2p and AES) XP parameters observed for CuC and CuCZ samples.

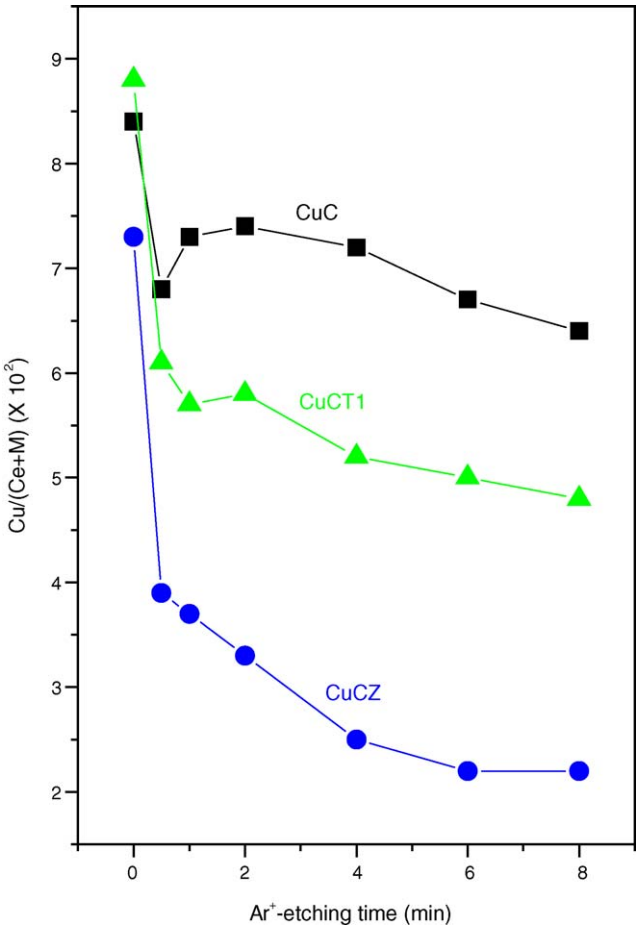

Fig. 4. Profile of the Cu/(Ce + M), M = Zr or Tb, atomic ratio as a function of the Ar^+-sputtering time for the indicated samples.

of CO_2 and/or H_2O in the reactant mixture has been analysed for the most active CuC catalyst. Taking as a reference, the maximum conversion temperature range (410–440 K), it is observed that introduction of 15% CO_2, 10% H_2O or 15% CO_2 + 10% H_2O in the CO + O_2 + H_2 reactant mixture produces a small drop in the CO conversion values to ca. 97, 93 and 87%, respectively, while the influence on the selectivity is relatively low except in the presence of both CO_2 and H_2O, in which case it decreases from 42 to 32%.

In order to analyse in detail the processes taking place over the samples in the course of the catalytic reaction, the CuC, CuCZ and CuCT1 samples have been analysed by *operando*-DRIFTS. Fig. 6 shows the results obtained under CO + O_2 + H_2 for the most active CuC catalyst. Bands are observed to be basically formed in three spectral zones. A first one corresponds to hydroxyl species (isolated ones giving sharp bands in the 3700–3600 cm^{-1} range and associated species giving a broad band extending from ca. 3800 to 3000 cm^{-1} [33]). Its formation, which could be related to direct hydrogen dissociation and further spillover processes and/or to chemisorption of water produced by H_2 oxidation, evidences the occurrence of hydrogen reaction. A second zone corresponds to carbonate-related species. Most intense peaks in this zone are related to bidentate carbonates at ca. 1586, 1297, 1033 and 854 cm^{-1} – a combination band at ca. 2883 cm^{-1} being related to these too – or monodentate carbonates showing the symmetric and antisymmetric stretching of the carboxylate group at ca. 1478 and 1399 cm^{-1}. Weak bands or shoulders at 1680 cm^{-1}, observed at T < ca. 373 K, reveal the formation of bridging carbonates, while those at ca. 1587 and 1356 cm^{-1} – along with those appearing at 2935 and 2845 cm^{-1} – indicate the formation of formate species for T > ca. 423 K [34,35]. The third (intermediate) spectral zone shows the formation of carbonyl species (a Cu^+-carbonyl giving rise to a band at ca. 2120–2110 cm^{-1}—assignment according to previous reports, in which details can be found [12,13,36]). The evolution of CO_2 (g) bands in the course of the run is also observed in this spectral zone. Comparison with the spectra obtained under the same conditions for the copper-free ceria support, CuCT1 and CuCZ (for which some representative spectra are displayed in Fig. 7) reveals the similarity in the type of species formed for the three sam-

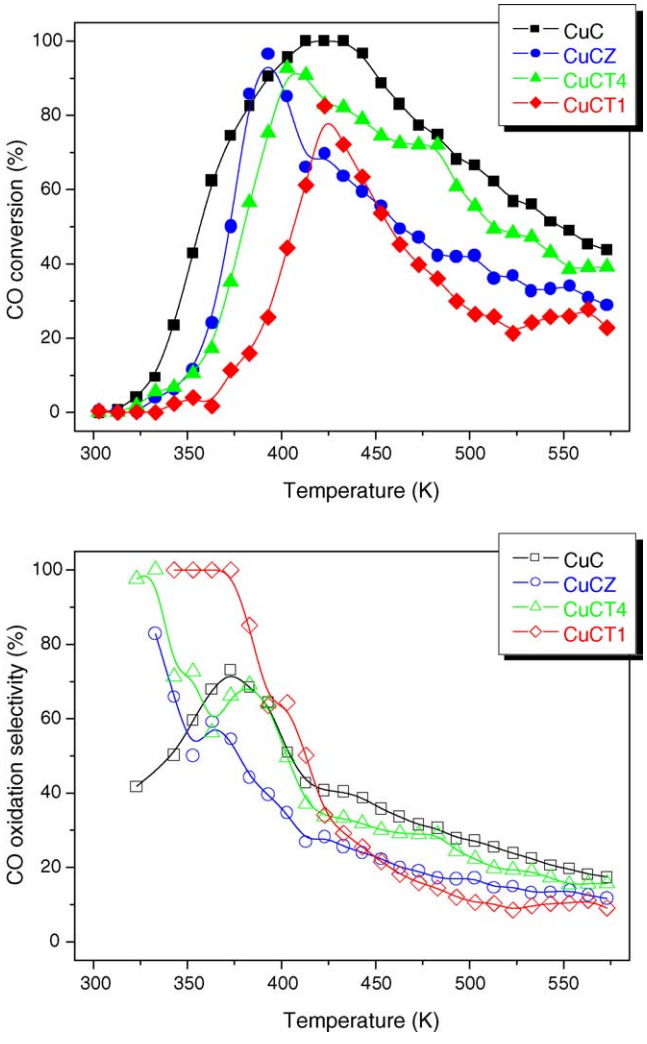

Fig. 5. Profiles of CO conversion (top) and selectivity for the CO PROX process (bottom) obtained during catalytic tests under 1% CO + 1.25% O_2 + 50% H_2 (Ar balance) for the indicated catalysts.

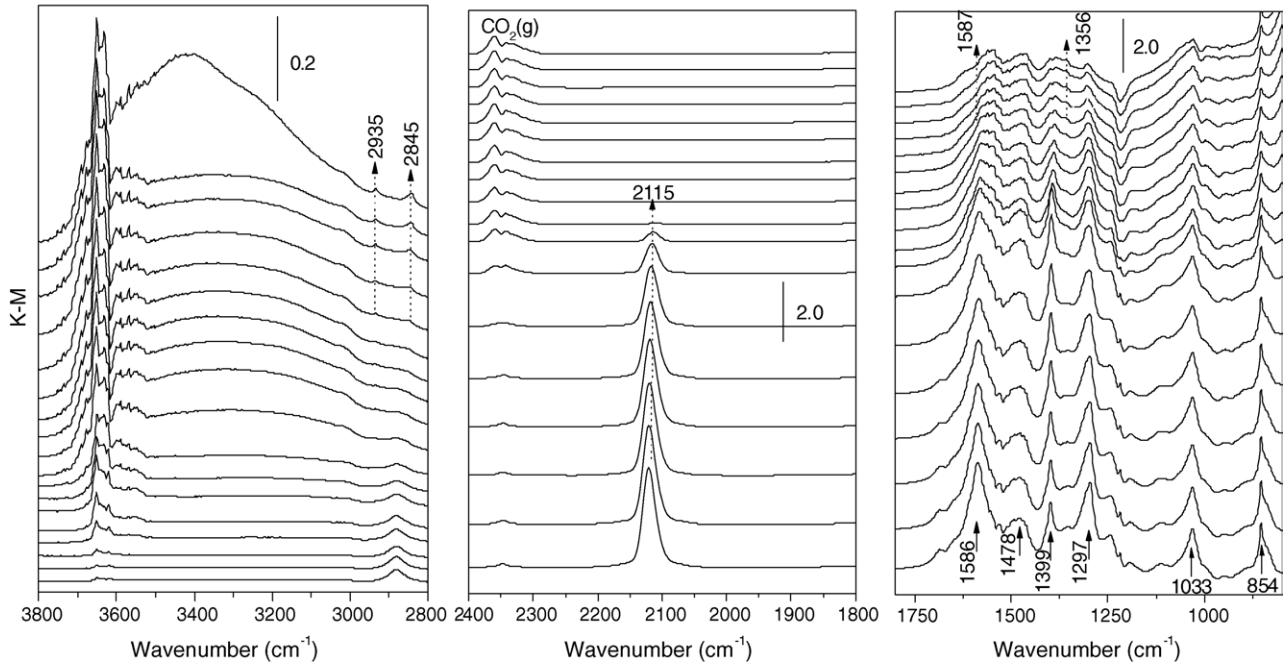

Fig. 6. DRIFTS spectra of CuC subjected to 1% CO + 1.25% O_2 + 50% H_2 in Ar between 303 and 473 K in steps of 10 K (from bottom to top). The spectrum of the initial sample calcined in situ under diluted O_2 has been subtracted in all cases.

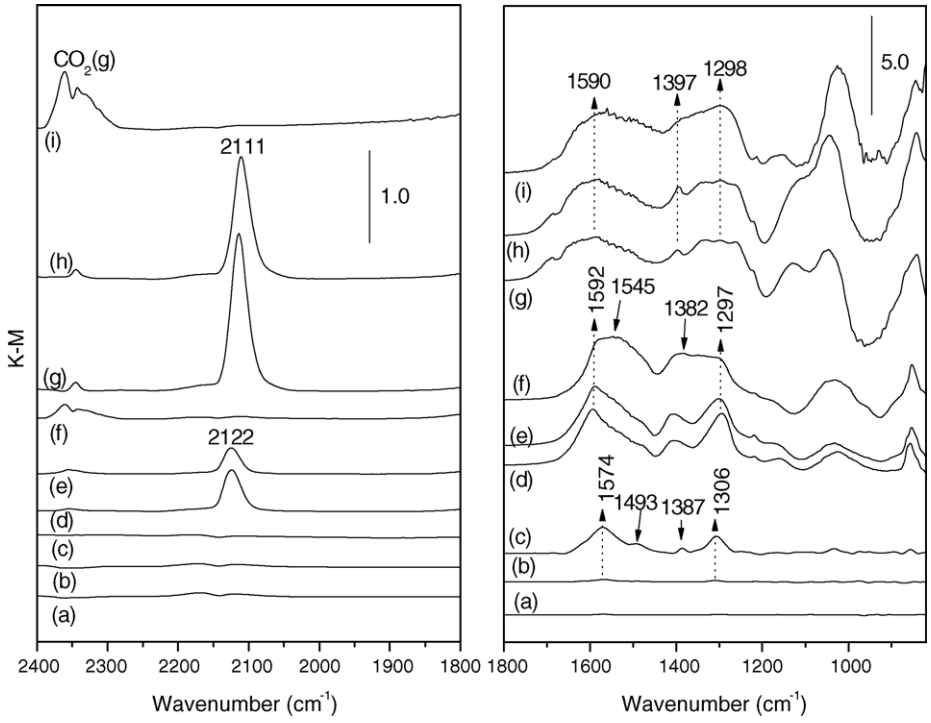

Fig. 7. DRIFTS spectra under 1% CO + 1.25% O_2 + 50% H_2 in Ar for the CeO_2 support (a–c), CuCT1 (d–f) and CuCZ (g–i) samples at 303 K (a, d, g), 363 K (b, e, h) and 453 K (c, f, i). The respective spectrum recorded prior to introduction of the reactant mixture (calcined in situ under diluted O_2 at 773 K) has been subtracted in all cases.

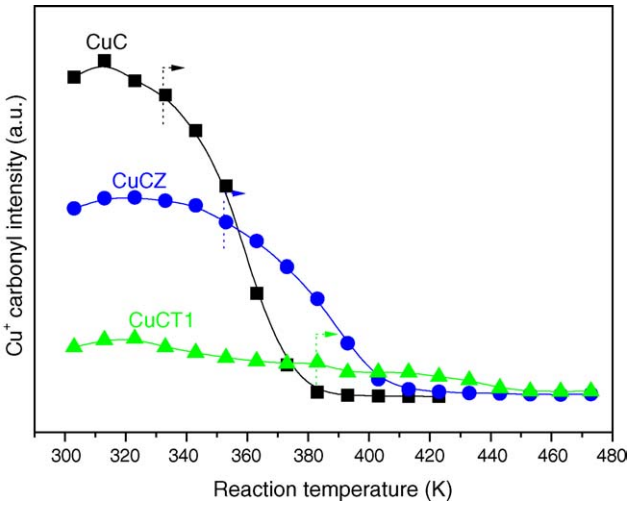

Fig. 8. Intensity of the Cu^+-carbonyl species (see text) detected by DRIFTS for the indicated samples in the course of the run under 1% CO + 1.25% O_2 + 50% H_2 in Ar. Dotted lines and arrows mark the onset of CO conversion in each case (see Fig. 9).

ples. Nevertheless, some differences are noteworthy. Thus, while the carbonate-related species formed for copper-free ceria appear fairly similar to those detected for CuC (basically bidentate species giving most intense bands at 1574 and 1306 cm^{-1} and monodentate ones at 1493 and 1387 cm^{-1}; note there is a certain shift in these values with respect to those observed for CuC), they begin to appear at comparatively higher temperature in the absence of copper, thus revealing a promoting effect of copper oxide on its formation and its possible location at ceria positions at or close to the oxide–oxide interface (which would explain the shift in bands positions). Relatively lesser differences are detected in this respect when comparing the three copper-containing samples, with most intense bands observed for CuCT1 and CuCZ being also related to various carbonate species. Significant differences are, however, detected between these samples with respect to the intensity of the Cu^+-carbonyl species (Fig. 7 shows representative spectra of this species appearing at a frequency similar than observed for CuC, for CuCT1 and CuCZ). As shown in Fig. 8, a correlation is noted between the activity for CO conversion and the intensity of the Cu^+-carbonyl. Note that points below reaction onset must generally be considered for this analysis, since such intensity can be affected by the CO conversion rate (while thermal stability should not be of relevancy in this respect at least for $T < 323$ K, irrespective of the support employed [12,13,36]).

In particular, the correlation evidenced in Fig. 8 points towards the redox activity of the corresponding CuO_x–$(Ce,M)O_x$ interfaces as the main factor determining the CO conversion catalytic behaviour during the PROX process. It must be noted that formation of the Cu^+-carbonyl must be related to a reduction process taking place under the reactant atmosphere, taking into account, as demonstrated above, the fully oxidized character of the initial samples. It may be argued that small amounts of reduced copper species (giving rise to the corresponding carbonyl species upon CO chemisorption) could be stabilized at the surface of the samples even for the initial calcined state of them [37]. It must, however, be considered the high reducibility of this type of $(Ce,M)O_x$-interacting copper oxide species, according to previous works in which (mainly on the basis of XPS and EPR evidences) ca. 70% of copper can be reduced to Cu^+ by CO at 300 K for CuC (while relatively lower redox activity was noted for CuCZ). Such strong facility for copper oxide reduction must be related to interfacial effects, i.e. promoted (differentially) by the corresponding support. This is based on the fact that, on the one hand, no significant reduction of bulk CuO by CO appears to proceed until $T >$ ca. 473 K [38]. On the other hand, the observed reducibility order between the catalysts (according to Fig. 8 but also considering previous analysis in this respect of CuC and CuCZ [11]) do not correlate with copper oxide dispersion levels inferred from the results of Fig. 4 (see above), while unsupported copper oxide particles would be expected to exhibit higher reducibility with decreasing their size [39]. This latter would be probably related with the higher facility for activation of reductant molecules in the presence of more defective copper oxide structures [38,40], which are most likely to appear generally as particle size is decreased to the nanometre range in oxide materials [41]. Therefore, as pointed out at the beginning of this paragraph, on these bases and irrespective on whether oxidising or reducing steps are rate determining in the CO oxidation mechanism (the rate of the former would, in principle, be proportional to the reduction level achieved in each case [11,12]), the results of Fig. 8 and the lack of significant differences concerning other type of species detected during the *operando*-DRIFTS experiments (most likely both carbonate-type and hydroxyls species are just spectators, although their unavoidable stabilization in this type of systems – at positions close to or at the active oxide–oxide interface – probably hinders to some extent their redox activities [14]) suggests that the catalytic behaviour for CO oxidation under CO-PROX conditions (whose rate mainly determines the overall performance of the whole CO PROX process [1]) is essentially related to the redox activity of the corresponding CuO_x–$(Ce,M)O_x$ interfaces. It must be also noted, as another potential factor that could affect catalytic activity of this type of systems, the difficulties to determine possible specific structural differences induced by the respective supports on the highly interacting copper oxide species in each case.

Fig. 9 shows the evolution of O_2 conversion in the course of the different catalytic tests performed with the DRIFTS cell reactor. First to be noted, the order of catalytic activity observed for the three samples (i.e. CuC > CuCZ > CuCT1) is the same for CO oxidation and H_2 oxidation reactions, suggesting that both reactions are dominated by the specific properties of the respective CuO_x–$(Ce,M)O_x$ interfaces, as discussed in the former paragraph, and/or by parallel effects induced by CuO_x-$(Ce,M)O_x$ interactions in each case. On the

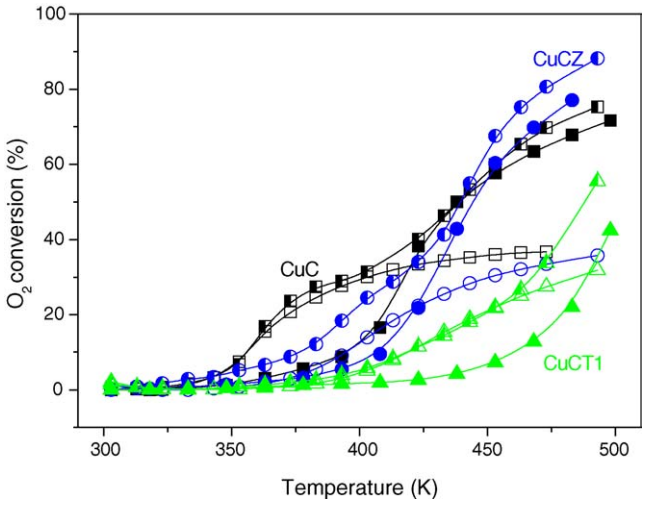

Fig. 9. O_2 conversion values obtained during *operando*-DRIFTS tests for the indicated catalysts under 1% CO + 1.25% O_2 + 50% H_2 (half-filled symbols), 1% CO + 1.25% O_2 (open symbols) and 1.25% O_2 + 50% H_2 (full symbols).

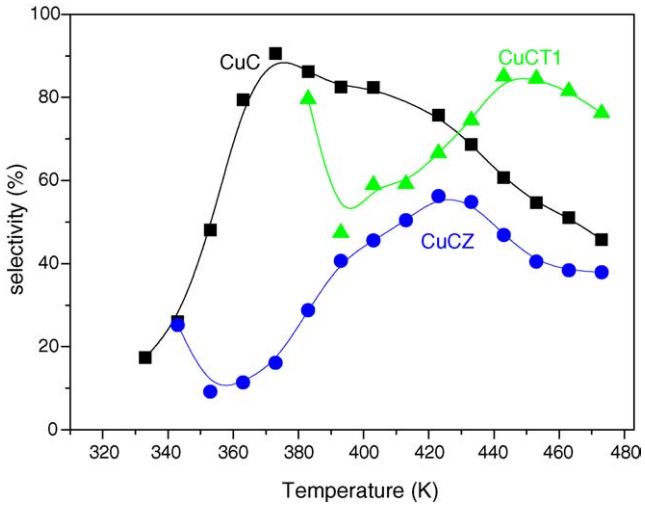

Fig. 10. Selectivity for the CO oxidation reaction observed during *operando*-DRIFTS tests under 1% CO + 1.25% O_2 + 50% H_2 for the indicated catalysts.

other hand, the profiles obtained under CO + O_2 + H_2 show for all cases basically two well differentiated zones, which, on the basis of comparison with the evolutions observed for oxidation of the individual CO or H_2 reductants, suggests that those are related to basically CO (lower T zone) and H_2 (higher T zone) oxidation processes. However, joint analysis of O_2 and CO_2 evolutions in the course of the *operando*-DRIFTS runs under CO + O_2 + H_2 shows that hydrogen oxidation is also involved in the lower T region, the selectivity profiles shown in Fig. 10 being extracted from this analysis. These confirm in general terms, the results obtained with the catalytic reactor shown in Fig. 5; differences must be due to the different characteristics of the reactor and/or the operating mode employed in each case. Thus, an intermediate maximum in the selectivity for CO oxidation is detected during any of the runs. Such maximum must essentially be related to the balance between a certain CO promotion of H_2 oxidation at low temperature (at temperatures below the maximum) and the differential rates of H_2 oxidation with respect to CO oxidation, the former being most favoured at high temperatures (at temperatures above the maximum). The low temperature effect appears to be more pronounced for CuC, giving rise to a steeper selectivity profile for this sample while it appears to be activated only at higher temperatures for the other samples (in particular during catalytic tests shown in Fig. 5). In fact, the magnitude of the effect appears to be related to the redox activity of the respective catalysts, considering discussion in a previous paragraph. This suggests that hydrogen oxidation is particularly promoted by formation under the reactant atmosphere of reduced states of copper (basically Cu^+ states) that could favour activation of the hydrogen molecules. In this sense, it must be noted the higher copper oxide reducibility observed for this type of systems under CO with respect to H_2, according to results in the literature [2]; in turn, previous results have suggested the existence of an interfacial reductive induction (involving copper oxide reduction) prior to onset of CO oxidation [12].

It may be, however, noted that the poorest overall selectivity is detected for CuCZ in any of the catalytic reactors (Figs. 5 and 10). This must be essentially related to the differential rates between CO and H_2 oxidation reactions, the latter being particularly most favoured for this system. In fact, this is basically reflected by the differences in the individual CO or H_2 oxidation rates inferred from oxygen evolutions shown in Fig. 9. A correlation can be established between these results and the copper oxide dispersion levels extracted from analysis of Fig. 4, which suggests that (within any particular system of this type, in which overall performance is mainly determined by its particular interfacial redox properties, as discussed before) H_2 oxidation is relatively favoured with respect to CO oxidation upon decreasing the size of the copper oxide particles; in this respect, previous results on bulk CuO systems indicate the easier H_2 activation in the presence of defective structures [40], which could be favoured upon decreasing particle size [41]. It must be mentioned that this hypothesis correlating CuO particle size with selectivity in the CO-PROX process was previously pointed out by Wang et al. on the basis of comparison of catalytic activity results obtained for CuO-samarium doped ceria samples in which samples with different specific areas were employed (from which it was tentatively assumed, as typically expected, an inversely proportional relation between copper oxide particle sizes and support surface area) [2]. Nevertheless, this hypothesis along with consideration of the interfacial effects on the overall catalytic performance suggests that an optimum intermediate CuO particle size can be achieved and yield optimum CO-PROX systems of this kind. Further experiments are, however, required, and in course in our laboratories, to corroborate these hypotheses.

4. Conclusions

Support effects have been revealed during preferential oxidation of CO in a H_2-rich stream over catalysts of copper oxide supported on ceria and Ce–M (M = Zr or Tb) mixed oxides. These include differences in the performances for CO and H_2 oxidation reactions (the ceria-supported system showing superior activity, while the systems supported on Ce–Tb mixed oxides display the lowest activities) and in the selectivity for CO oxidation (the Ce–Zr-supported system showing the lowest selectivity in global terms). Support effects for conversion of the reductants are correlated, mainly on the basis of *operando*-DRIFTS results, with redox activities of the corresponding interfaces between highly dispersed copper oxide entities (evidenced by XAFS and XPS) and the support in each case. Details of the selectivity for the CO-PROX process include observation of an intermediate temperature maximum attributed to the balance between a low-temperature CO promotion of H_2 oxidation (differentially activated as a function of the support, the effect being most pronounced for the ceria-supported system) and differences in the respective CO and H_2 oxidation rates essentially determining the high temperature selectivity. While the former process is proposed to be connected to the interfacial redox activity (being thus most favoured for the ceria-supported system), effects of copper oxide particle size (differences being based on qualitative dispersion estimations obtained by means of XPS Ar^+-sputtering experiments) are proposed to be relevant for the respective H_2 oxidation activities thus affecting significantly the selectivity at high temperature and the overall selectivity for the CO-PROX process.

Acknowledgements

Thanks are given to Ms. A. Iglesias-Juez and to the scientific and technical staff at Daresbury Laboratory Station 9.3 (Drs. A.R. Lennie and I. Harvey) for the help given during recording of the XAFS spectra. Thanks are also due to ICP-Unidad de Apoyo staff for chemical analysis results and XRD recording and to Mr. A. Macías for assistance in recording XPS data. Financial help by CICyT Project MAT2003-03925 is acknowledged.

References

[1] G. Avgouropoulos, T. Ioannides, C. Papadopoulou, J. Batista, S. Hocevar, H.K. Matralis, Catal. Today 75 (2002) 157.
[2] J.B. Wang, S. Lin, T. Huang, Appl. Catal. A 232 (2002) 107.
[3] G. Sedmak, S. Hocevar, J. Levec, J. Catal. 213 (2003) 135.
[4] D.H. Kim, J.E. Cha, Catal. Lett. 86 (2003) 107.
[5] O. Korotkikh, R. Farrauto, Catal. Today 62 (2000) 249.
[6] M. Watanabe, H. Uchida, K. Ohkubo, H. Igarashi, Appl. Catal. B 46 (2003) 595.
[7] M. Shou, K.-I. Tanaka, K. Yoshioka, Y. Moro-oka, S. Nagano, Catal. Today 90 (2004) 255.
[8] A.F. Ghenciu, Curr. Opin. Sol. St. Mater. Sci. 6 (2002) 389.
[9] M.M. Schubert, A. Venugopal, M.J. Kahlich, V. Plzak, R.J. Behm, J. Catal. 222 (2004) 32.
[10] A. Luengnaruemitchai, S. Osuwan, E. Gulari, Int. J. Hydrogen Energy 29 (2004) 429.
[11] A. Martínez-Arias, M. Fernández-García, O. Gálvez, J.M. Coronado, J.A. Anderson, J.C. Conesa, J. Soria, G. Munuera, J. Catal. 195 (2000) 207.
[12] A. Martínez-Arias, M. Fernández-García, A.B. Hungría, A. Iglesias-Juez, O. Gálvez, J.A. Anderson, J.C. Conesa, J. Soria, G. Munuera, J. Catal. 214 (2003) 261.
[13] A. Martínez-Arias, M. Fernández-García, J. Soria, J.C. Conesa, J. Catal. 182 (1999) 367.
[14] A. Trovarelli (Ed.), Catalysis by Ceria and Related Materials, Imperial College Press, 2002.
[15] A.B. Hungría, A. Martínez-Arias, M. Fernández-García, A. Iglesias-Juez, A. Guerrero-Ruiz, J.J. Calvino, J.C. Conesa, J. Soria, Chem. Mater. 15 (2003) 4309.
[16] A. Martínez-Arias, M. Fernández-García, A.B. Hungría, J.C. Conesa, G. Munuera, J. Phys. Chem. B 107 (2003) 2667.
[17] M.D. Hernández-Alonso, A.B. Hungría, A. Martínez-Arias, J.M. Coronado, J.C. Conesa, J. Soria, M. Fernández-García, Phys. Chem. Chem. Phys. 6 (2004) 3524.
[18] A. Martínez-Arias, M. Fernández-García, V. Ballesteros, L.N. Salamanca, J.C. Conesa, C. Otero, J. Soria, Langmuir 15 (1999) 4796.
[19] J.F. Ziegler, J.P. Biscrock, The Stopping and Range of Ions in Solids, Pergamon Press, 1995, p. 578.
[20] R. Hesse, T. Chassé, R. Szargan, Fresenius J. Anal. Chem. 365 (1999) 48.
[21] C.D. Wagner, W.M. Riggs, L.E. Davis, J.F. Moulder, in: G.E. Muilenberg (Ed.), Handbook of X-ray Photoelectron Spectroscopy, first ed., Perkin-Elmer Corporation (Physical Electronics), 1979.
[22] J.P. Holgado, R. Alvarez, G. Munuera, Appl. Surf. Sci. 161 (2000) 164.
[23] S.M.L. Schroeder, G.D. Modrigge, R.M. Lambert, T. Rayment, in: R.J.H. Clark, R.E. Hester (Eds.), Spectroscopy for Surface Science, Wiley, NY, 1998 (Chapter 1).
[24] X.D. Zhou, W. Huebner, Appl. Phys. Lett. 79 (2001) 3512.
[25] X. Wang, J.C. Hanson, G. Liu, J.A. Rodriguez, A. Iglesias-Juez, M. Fernández-García, J. Chem. Phys. 121 (2004) 5434.
[26] A. Martínez-Arias, A.B. Hungría, M. Fernández-García, J.C. Conesa, G. Munuera, J. Phys. Chem. B 108 (2004) 17983.
[27] C. Márquez-Alvarez, I. Rodríguez-Ramos, A. Guerrero-Ruiz, G.L. Haller, M. Fernández-García, J. Am. Chem. Soc. 119 (1997) 2905.
[28] S.-F. Cheah, G.E. Brown Jr., G.A. Parks, J. Colloid Interface Sci. 208 (1998) 110.
[29] J.P. Espinós, J. Morales, A. Barranco, A. Caballero, J.P. Holgado, A.R. González-Elipe, J. Phys. Chem. B 106 (2002) 6921.
[30] A.R. González-Elipe, J.P. Espinós, A. Fernández, G. Munuera, in: H.H. Brongersma, R.A. van Santen (Eds.), Fundamental Aspects of Heterogeneous Catalysis Studied by Particle Beams (NATO ASI Series C 27), Plenum Press, NY, 1991.
[31] A.R. González-Elipe, J.P. Holgado, R. Alvarez, J.P. Espinós, A. Fernández, G. Munuera, J. Catal. 130 (1991) 627.
[32] Y. Li, Q. Fu, M. Flytzani-Stephanopoulos, Appl. Catal. B 27 (2000) 179.
[33] A. Badri, C. Binet, J.C. Lavalley, J. Chem. Soc. Faraday Trans. 92 (1996) 4669.
[34] C. Li, Y. Sakata, T. Arai, K. Domen, K.-I. Maruya, T. Onishi, J. Chem. Soc. Faraday Trans. 1 (85) (1989) 929.
[35] C. Li, Y. Sakata, T. Arai, K. Domen, K.-I. Maruya, T. Onishi, J. Chem. Soc. Faraday Trans. 1 (85) (1989) 1451.
[36] A. Martínez-Arias, R. Cataluña, J.C. Conesa, J. Soria, J. Phys. Chem. B 102 (1998) 809.
[37] W. Liu, A.F. Sarofim, M. Flytzani-Stephanopoulos, Chem. Eng. Sci. 49 (1994) 4871.

[38] X. Wang, J.C. Hanson, A.I. Frenkel, J.-Y. Kim, J.A. Rodriguez, J. Phys. Chem. B 108 (2004) 13667.
[39] C.L. Carnes, K.J. Klabunde, J. Mol. Catal. A 194 (2003) 227.
[40] J.Y. Kim, J.A. Rodriguez, J.C. Hanson, A.I. Frenkel, P.L. Lee, J. Am. Chem. Soc. 125 (2003) 10684.
[41] M. Fernández-García, A. Martínez-Arias, J.C. Hanson, J.A. Rodriguez, Chem. Rev. 104 (2004) 4063.